Dynamics of precipitation pattern formation at geothermal hot springs

Nigel Goldenfeld, Pak Yuen Chan and John Veysey
Department of Physics, University of Illinois at Urbana-Champaign,
Loomis Laboratory of Physics, 1110 West Green Street, Urbana, Illinois, 61801-3080.

We formulate and model the dynamics of spatial patterns arising during the precipitation of calcium carbonate from a supersaturated shallow water flow. The model describes the formation of travertine deposits at geothermal hot springs and rimstone dams of calcite in caves. We find explicit solutions for travertine domes at low flow rates, identify the linear instabilities which generate dam and pond formation on sloped substrates, and present simulations of statistical landscape evolution.

PACS numbers: 05.45.Ra, 87.23.n, 47.54.-r, 89.75.Kd, 47.20.Hw, 47.15.gm, 47.55.np

The terraced architecture of carbonate mineral deposits at geothermal hot springs is one of the most striking and beautiful terrestrial landscapes. Spring water at above 70^{o}C emerges from the ground at a vent, releases CO_2 and precipitates $CaCO_3$ in the form of travertine, as it flows downhill over the pre-existing terrain[1, 2, 3]. The terrain itself is thus constantly changing in response to the influx of $CaCO_3$, with measurements indicating precipitation rates as high as 1-5 mm per day[4, 5, 6]. The ever-changing substrate modifies the flow path of the spring water, resulting in a constant dynamic interplay between the landscape and the fluid flow as the travertine outcrop develops and grows. The resulting morphology is a cascade of nested ponds and terraces at a wide variety of scales ranging from hundreds of meters down to millimeters, as shown in Fig. (1).

Most studies of this phenomenon have tended to focus on the microscopic origins of the crystal growth process: what is the extent of biomineralization due to thermophilic microbes[6, 7]?; what are the primary controls on degassing[8, 9], mineral composition[10, 11], crystal fabric and habit[12], and structure[13, 14]? These issues are complex and system dependent, but a main theme is the competition between biotic and abiotic mechanisms of precipitation. Microbial metabolic activity can in principle locally influence the CO_2 composition of the water column, thereby affecting the rate of $CaCO_3$ precipitation. However, turbulent flow over pond lips or evaporation can be more effective degassing mechanisms[9]. In fact, the issue of biotic versus abiotic mechanism is not straightforward, because even if the main mechanism for degassing is abiotic, the kinetics of precipitation and crystal growth may require the presence of exogenous particles (such as dead or living bacteria) to initiate nucleation.

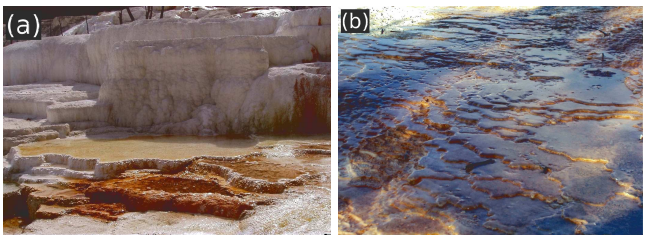

FIG. 1: (Color online) Travertine formation at Angel Terrace, Mammoth Hot Springs, WY. (a) a large pond, of order 1 meter in diameter, and smaller features. (b) a portion of the flow system about 25 meters from the vent, on the scale of centimeters.

The purpose of this Letter is to address instead the origin of the large scale structure of the terraced architecture. The ubiquity of this morphology at carbonate geothermal hot springs world-wide, as well as at low temperature speleothem rimstone dam formations[15], suggests that it is appropriate to seek a generic explanation based on principles of fluid dynamics, precipitation kinetics, and crystal growth dynamics, rather than one that hinges on specific material parameters or system components such as microbes. In fact, we will see that it is possible to explain in this way the formation of ponds, the variations in terrace morphology, the absence of an obvious characteristic lengthscale of the landscape, and even the quantitative properties of simple landscape motifs, such as the circularly-symmetric travertine dome shown in Fig. (2a).

The formation of a terraced architecture is a result of a depositional instability arising from turbulent flow of a supersaturated solution over a surface, and represents an example of free boundary dynamics in precipitative pattern formation, related to the phenomena that give rise to stalactites[16, 17].

Travertine domes:- We begin by analyzing the dynamics of pattern motifs, ignoring interactions between them, by analogy with earlier work on solidification patterns[18]. In the present problem, these features are pond lips[19] and travertine domes.

We now formulate a boundary-layer model[18] of the growth of travertine domes, coupling the evolution of the travertine substrate to the fluid dynamics in a thin film of depth h around it. The kinematic equation governing time evolution of the curvature, κ, of a curve in two dimensions is given by[18, 20]:

$$\left.\frac{\partial \kappa}{\partial t}\right|_{\theta} = -\kappa^2 \left(1 + \frac{\partial}{\partial \theta^2}\right) v_n, \qquad (1)$$

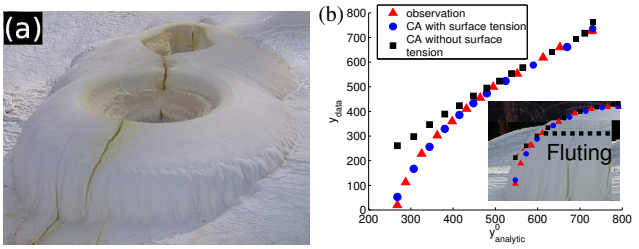

FIG. 2: (Color online) Travertine dome at Mammoth Hot Springs, WY. (a) Dome whose central pond is 50.3cm in diameter. (b) Dome height as a function of θ. Horizontal axis: analytical prediction from Eq. (4). Vertical axis: simulated dome (CA) with no surface tension (squares), with surface tension (circles), and the profile of the dome in (a) (triangles, data digitized from photograph). The points all fall on a straight line with unit slope above the fluting point, indicating agreement with Eq. (4) fitting only r_0. Below that one extra parameter is required, as explained in the text. Inset: comparison with dome from (a).

where θ is the angle between the surface and the vertical axis and v_n is the normal growth velocity of the surface. The time derivative in the equation is defined with respect to fixed θ. This equation is purely geometrical; for any given function v_n of water chemistry, surface kinetics, fluid flow state, the evolution of κ is determined. Here, we follow Wooding[19] and make the simple assumption that v_n is directly proportional to the depth-averaged tangential fluid velocity U: $v_n = GU$ where G is a mass transfer coefficient, depending on the water chemistry and the turbulent flow near the growing surface[21].

In general, we need to couple the Navier-Stokes equation to Eq. (1) to obtain a complete description of the coupled fluid dynamics and surface kinematics, but there are a number of simplifications. First, because the growth rate is of order $1-5$mm/day and the fluid flow rate is of order 1mm/sec, there is a separation of time scales. So if we are interested in the morphological evolution, we can neglect the change in flow rate, represented by the time derivative in the Navier-Stokes equation. Second, our field observations indicate that the thickness of the fluid film flowing over the domes is very small compared to the curvature of the surface; thus, we make the approximation that the fluid is flowing down a (locally) constant slope. In addition, the flow is apparently laminar, so that we can use the Poiseuille-Hagen profile for the velocity in thin film to give a depth-averaged mean flow velocity U:

$$U = \left(\frac{\alpha \sin\theta}{r^2}\right)^{1/3}, \tag{2}$$

where $\alpha \equiv gQ^2/12\pi\nu$, g is the gravitational acceleration, Q is the total mass flux coming out of the vent, ν is the viscosity of the fluid and r is the axial distance from the vent. Circular symmetry is imposed to arrive at (2). We will later see that the assumption of laminar flow is self-consistently verified. For a dome, steadily translating upwards without change of shape with velocity v_t, Eq. (1) gives

$$G\left(\frac{\alpha \sin\theta}{r^2}\right)^{1/3} = v_t \cos\theta, \tag{3}$$

Rearranging terms gives the shape of the dome as a one-parameter family of curves

$$r(\theta)/r_0 = \sqrt{\frac{\sin\theta}{\cos^3\theta}}. \tag{4}$$

where the scale factor $r_0 \equiv \sqrt{G^3\alpha/v_t^3}$. Eq. (4) is plotted in Fig. (2b). Good agreement is obtained between our theory and the observations below a critical angle θ_c. From the fit, and the typical parameter values $G \sim 10^{-8}$, $v_t \sim 1$mm/day and $Q \sim 1\text{cm}^3$/sec, we obtain $U \sim 25$mm/sec and $h \sim 1-10$mm, and a Reynold's number, $\text{Re} \equiv Uh/\nu \sim 10-100$. The assumption of laminar flow is self-consistently verified.

For angles $\theta > \theta_c$, the analytical profile does not fit the field observations; the point of departure closely follows the point where we also observe a fluting pattern around the dome. We will show below that this is due to the effects of surface tension at the air-water-travertine interface. As the water flows out of the dome, it is spread over an increasingly larger area and thus the fluid thickness decreases, ultimately reaching a point where contact lines form and surface tension can not be ignored. The analytical solution above neglects surface tension, but is able to predict the limiting point of its validity when $h \sim d_c$, leading to a prediction for the scaling dependence of the critical angle on the model parameters.

The inclusion of surface tension introduces an additional length scale, namely, the capillary length, d_c, into the problem. Now, the only other length scale in the problem is $r_0 = \sqrt{gG^3Q^2/\nu v_t^3}$. Since θ_c is dimensionless, it can only depend on the ratio r_0/d_c and G. For a given chemical environment, G is fixed and we are left with the prediction, derived from our analytical solution, that

$$\theta_c = \hat{f}(\sqrt{(gQ^2/\nu v_t^3)}/d_c), \tag{5}$$

verified below in Fig. (3b).

The damming instability:- To understand the lack of any characteristic scale in the landscape, we consider the stability of the moving boundary problem for turbulent fluid flowing down a constant slope, on which deposition may occur. In order to capture the turbulent flow, we make two approximations. First, we use the thin film approximation attributed to de St. Venant, which is valid when the fluid film thickness is much less than the characteristic scale of variation of the flow in the streamwise direction, but include the lowest order corrections for the

curvature of the underlying surface[22, 23].

$$\begin{array}{lcl} \partial_t u_0 + \partial_s E & = & -C_f g u^2/gh(1-\kappa h) \\ (1-\kappa h)\partial_t h - \partial_s q & = & 0 \end{array} \quad (6)$$

where

$$\begin{array}{lcl} u(s,n,t) & = & u_0(s,t)/(1-\kappa h), \\ E(s,t) & = & \zeta + h\cos\theta + u_0^2/(2g(1-\kappa h)^2), \\ q(s,t) & = & -u_0/(\kappa \log(1-\kappa h)), \end{array} \quad (7)$$

where u is the fluid velocity, h is the fluid thickness, ζ is the height of the underlying surface measured from a fixed horizontal axis and s is the arc length measured from the top of the system. Secondly, we have modeled turbulent flow phenomenology by including the term proportional to C_f, the Chézy coefficient[24], which empirically describes the energy lost due to turbulence, in a manner consistent with Kolmogorov's 1941 scaling theory of turbulence (K41)[25, 26]. These two equations have to be solved together with the growth equation (1). The trivial solution to this set of equations can be easily found, and is simply uniform viscous flow down a slope.

To study the linear stability of this solution, we add a perturbation proportional to $\exp(ikx + \omega(k)t)$, and calculate the spectrum of the growth rate ω as a function of the wavenumber k for the linearised set of equations. It is found that $\mathrm{Re}(\omega)$ is positive for all values of k, indicating that the system is unstable towards perturbations of all length scales, with no special scale singled out at linear order.

We next present an approach to simulate the statistical correlations of the terraced landscape in the fully-nonlinear regime.

Cellular modeling:- We represent the landscape as composed of stacked "bricks" or cells by its height $H(i,j)$, above a horizontal reference plane, where i and j are $x-y$ coordinates in the reference plane. The water column is situated above the height field and represented by the variable $W(i,j)$ describing the volume of water above each coordinate element. Each packet of water can also contain calcium ions, $C(i,j)$, and dissolved carbon dioxide vapor, $V(i,j)$, which may potentially cause precipitation through a caricature of the complex reaction pathway given by $Ca^{2+} + 2HCO_3^- \rightleftharpoons CaCO_3(s) + H_2O + CO_2(g)$. The evolution of the landscape is governed by update rules on these fields, which mimic and go beyond the continuum description given above. In addition, at each point, it is necessary to keep track of water that is ponded, $W_p(i,j)$, and the temperature of the water $T(i,j)$.

A complete lattice update consists of the following steps, which we will describe in more detail below: (1) Add water to the system, at the spring source taken to be the origin; (2) Propagate all the water in the system, by moving packets to nearest and next nearest neighbour grid points, and ensuring that the water in all ponds is level; (3) Update the water chemistry, e.g. $C(i,j)$ and $V(i,j)$ to take into account outgassing due to fluid motion and depletion of Ca ions due to precipitation; (4) Evolve the height field in response to the precipitation of $CaCO_3$.

In step (1), a quantity of water δW is added at the source, so that $W'(0) = W_0$, a constant value appropriate for a constant pressure head (neglecting the change in pressure due to the vertical growth of the landscape). Here and below, primed quantities denote the updated variables. The new water added to the system contains initial concentrations of calcium, C_0, carbon dioxide, V_0, and is at a temperature T_0; the fact that the source water is undersaturated is represented by $C_0 < V_0$. The values of these fields at the source point are updated based on the volumetric ratio of the amount of water added to the existing water: e.g. $C' = (C(0)W(0) + \delta W C_0)/W_0$, and similarly for the CO_2 concentration and temperature fields.

The transport of water in step (2) is carried out by a variation of an algorithm used for braided river flow[27], in which the flux along bonds connecting a given lattice point to one of its eight closest neighbours is determined by the landscape gradient along that direction, while conserving the total volume of water. If the slope S exceeds a threshold S_c, the flow is taken to be turbulent and the flux is proportional to $\sqrt{S}$ in accord with Chézy's law. The appropriate height variable for determining the chemical potential of the water, and hence the equilibrium filling of ponds in the landscape is the "energy surface" $H_T \equiv H + W$. Water moving on this surface is also subject to surface tension and contact line effects, that can be important near the rim of a pond, for example[28]. This is modeled by requiring that water is propagated only if W exceeds a small threshold at that point. Packets of water carry with them advected variables T, C and V, which are updated by the volumetrically-weighted average of all the neighbourhood points from which the water packet originated.

Water chemistry is updated in step (3), by allowing a constant fraction of CO_2 to outgas at each time step, with an additional outgassing component proportional to $\sqrt{S}/(1+\sqrt{S})$ to reflect the influence of slope-initiated turbulent flow. As $CaCO_3$ is deposited, the concentrations C and V change to reflect mass balance.

The evolution of the height field H is the final step in the lattice update, with a change given by $\delta H = (C-V) \times (R_1 + R_2 \vec{F}\cdot\vec{n} + R_3(S))$. Here R_1 and R_2 are positive constants, $\vec{F}$ is the flux between cells, with a direction given by the component of the gradient of the energy surface H_T between cells and magnitude given by the volume of water propagation per unit time step, $\vec{n}$ is the unit vector normal to the underlying surface H, and $R_3(S)$ is proportional to $\sqrt{S}$, representing the increased precipitation due to Bernoulli effects and local turbulent

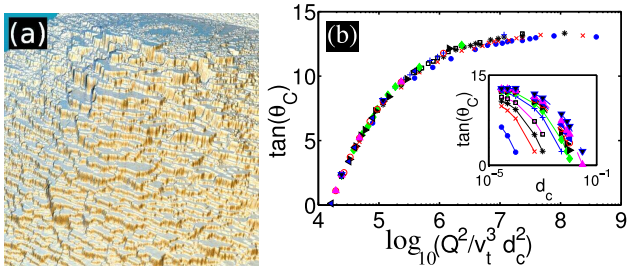

FIG. 3: (Color online) Results from simulation of the CDS model. (a) Portion of a typical simulated landscape. The figure clearly shows distinct geomorphological regimes or facies, as observed in the field[6]. (b) Critical angle for the contact line formation on a travertine dome, plotted according to Eq. (5), showing data collapse, as predicted by theory. Inset: raw data.

degassing.

In Fig. (3a) is shown a snapshot from a typical time-dependent simulation, initiated on a sloping plane with small initial roughness. For generic values of the model parameters, we observe the depositional instability predicted above, and the formation of ponds and terraces in broad qualitative agreement with field observations. The same calculation also yields travertine domes when initiated on an initially horizontal surface. Fig. (2b) shows that the CA model agrees with the analytical theory when the surface tension is switched off. Moreover, the same CA model predicts the exact shape of the observed travertine domes when surface tension is switched on, with a contact line at θ_c where fluting emerges. The scaling prediction Eq. (5) is verified in Fig. (3b) over 5 decades of $Q^2 v_t^3/d_c^2$; the inset shows the raw (unscaled) data for θ_c as a function of d_c for $v_t \sim 0.5$ and $0.1 < Q < 5000$. Our results show that travertine precipitation pattern formation results from an interplay between fluid flow, capillarity and chemistry, that can be captured quantitatively from both analytical and cell dynamical system approaches.

Future field work and extended simulation studies will explore the statistical properties of terraced landscapes, and whether these have a universal character computable with no adjustable parameters by minimal models. For example, layer fluctuations in ancient stromatolite rocks exhibit power-law correlations accurately captured by a simple generic model[29] in the same spirit as the one given here. Our preliminary simulations indicate that at least some statistical measures of the landscapes, such as the pond size distribution function, are fractal.

We acknowledge valuable discussions with Bruce Fouke and Michael Kandianis. We thank Nicholas Guttenberg for assistance with image rendering. This work was supported in part by the National Science Foundation through grant number NSF-EAR-02-21743.

[1] E. T. Allen and A. L. Day, Tech. Rep. publication 466, Carnegie Institute of Washington (1935).
[2] A. Pentecost and H. A. Viles, Geographie Physique et Quaternaire **48**, 305 (1994).
[3] T. D. Ford and H. M. Pedley, Earth Science Reviews **41**, 117 (1996).
[4] I. Friedman, Geochimica et Cosmochimica Acta **34**, 1303 (1970).
[5] A. Pentecost, Geol. Mag. **127**, 159 (1990).
[6] B. W. Fouke, J. D. Farmer, D. J. D. Marais, L. Pratt, N. C. Sturchio, and M. K. Discipulo, J. Sed. Res. **70**, 265 (2000).
[7] B. W. Fouke, J. Sed. Res. **71**, 497 (2001).
[8] J. S. Herman and M. M. Lorah, Chemical Geology **62**, 251 (1987).
[9] D. D. Zhang, Y. Zhang, A. Zhu, and X. Cheng, J. Sed. Res. **71**, 205 (2001).
[10] I. Barnes and J. R. O'Neil, Geochimica et Cosmochimica Acta **35**, 699 (1971).
[11] H. S. Chafetz, P. F. Rush, and N. M. Utech, Sedimentology **38**, 107 (1991).
[12] C. Buczynski and H. S. Chafetz, J. Sed. Petrology **61**, 226 (1991).
[13] E. Busenberg and L. N. Plummer, in *US Geological Survey, Bulletin 1578*, edited by F. A. Mumpton (1986), pp. 139–168.
[14] R. W. Renaut and B. Jones, Canadian Journal of Earth Sciences **34**, 801 (1996).
[15] J. Motyka, M. Gradziński, P. Bella, and P. Holúbek, Environmental Geology **48**, 682 (2005).
[16] M. B. Short, J. C. Baygents, J. W. Beck, D. A. Stone, R. S. T. III, and R. E. Goldstein, Phys. Rev. Lett. **94**, 018501 (2005).
[17] M. B. Short, J. C. Baygents, and R. E. Goldstein, Phys. Fluids **17**, 083101 (2005).
[18] E. Ben-Jacob, N. Goldenfeld, J. S. Langer, and G. Schon, Phys. Rev. Lett. pp. 1930–1932 (1983).
[19] R. A. Wooding, J. Geophysical Res. **96**, 667 (1991).
[20] R. C. Brower, D. A. Kessler, J. Koplik, and H. Levine, Phys. Rev. A **29**, 1335 (1984).
[21] J. A. Campbell and T. J. Hanratty, AlChE Journal **28**, 988 (1982).
[22] R. F. Dressler, J. Hydraul. Res. **16**, 205 (1978).
[23] N. S. Sivakumaran, R. Hosking, and T. Tingsanchali, J. Fluid Mech. **111**, 411 (1981).
[24] A. Chézy (1776), file No. 847, Ms. 1915 in the library of Ecole des Ponts et Chaussées. English translation in H. Clemens, On the origin of the Chézy formula, Journal Association of Engineering Societies, v. 18, pp. 363-369, (1897).
[25] A. N. Kolmogorov, Dokl. Akad. Nauk. SSSR **30**, 299 (1941), [English translation in Proc. R. Soc. London Ser. A 434 (1991)].
[26] K. R. Sreenivasan, Rev. Mod. Phys. **71**, S383 (1999).
[27] A. B. Murray and C. Paola, Nature **371**, 54 (1994).
[28] R. C. Kerr and J. S. Turner, J. Geophysical Res. **101**, 25125 (1996).
[29] J. P. Grotzinger and D. H. Rothman, Nature **383**, 423 (1996).